ChemComm

View Online
Dynamic Article Links

Cite this: *Chem. Commun.*, 2011, **47**, 9221–9223

www.rsc.org/chemcomm

COMMUNICATION

Hot-injection synthesis of iron/iron oxide core/shell nanoparticles for T_2 contrast enhancement in magnetic resonance imaging†

David A. J. Herman,[a] Peter Ferguson,[b] Soshan Cheong,[ac] Ian F. Hermans,[b] Ben J. Ruck,[a] Kathryn M. Allan,[a] Sujay Prabakar,[a] John L. Spencer,[a] Conrad D. Lendrum[c] and Richard. D. Tilley*[a]

Received 9th June 2011, Accepted 29th June 2011
DOI: 10.1039/c1cc13416g

Here we report a new, bench-top synthesis for iron/iron oxide core/shell nanoparticles *via* the thermal decomposition of Fe(η^5-$C_6H_3Me_4$)$_2$. The iron/iron oxide core/shell nanoparticles are superparamagnetic at room temperature and show improved negative contrast in T_2-weighted MR imaging compared to pure iron oxides nanoparticles, and have a transverse relaxivity (r_2) of 332 mM^{-1} s^{-1}.

Magnetic nanoparticles are an attractive area of research due to their size dependent magnetism and biomedical applications, such as magnetic hyperthermia, bioseparation and magnetic resonance imaging (MRI) contrast agents.[1] For MRI contrast agents, superparamagnetic nanoparticles are desired, to prevent aggregation occurring in the body when the applied magnetic field is removed.[2] Currently, superparamagnetic iron oxide nanoparticles (SPIOs) are the only commercially available negative contrast agents[2b] and are able to shorten T_2 relaxation times.[3,4] Reports show that materials with larger magnetizations, can induce further shortening of T_2 relaxation times resulting in greater MRI contrast enhancement.[5] Iron is ferromagnetic and has the highest saturation magnetization (218 emu g^{-1}) of the elements. Iron nanoparticles smaller than 15 nm are expected to be superparamagnetic.[6] The magnetic properties when coupled with the biocompatibility, make iron based nanoparticles ideal candidates for MRI contrast agents.[6,7] Development in this area remains challenging due to difficulty in obtaining stable iron nanoparticles from simple synthetic procedures and precursors.[7,8]

Under ambient conditions, iron nanoparticles smaller than 8 nm in size fully oxidize upon exposure to air.[9] Larger iron nanoparticles upon exposure to air form a 2–3 nm iron oxide shell on the surface, yielding iron/iron oxide core/shell nanoparticles. Successful studies for the synthesis of iron nanoparticles of sizes greater than 8 nm has been achieved *via* the decomposition of iron pentacarbonyl, Fe(CO)$_5$.[8,10] Other precursors such as iron oleate and iron bis(trimethylsilyl)amide have been used to achieve the formation of iron nanocubes.[11] However, the ease of nanoparticle synthesis and scalability is limited with these processes; Fe(CO)$_5$ is volatile and highly toxic,[7] other precursors are either air-sensitive,[11b] or require high temperature for decomposition.[11a] Recently, we have reported the synthesis of iron/iron oxide core/shell nanoparticles *via* the decompsition of an iron organometallic sandwich compound, Fe(C_5H_5)(C_6H_7), in a closed reaction vessel, under a hydrogen atmosphere.[12]

Here we report the bench-top synthesis of superparamagnetic iron/iron oxide core/shell nanoparticles *via* the thermal decomposition of a new, easy to handle, symmetrical iron organometallic sandwich compound, bis(η^5-1,3,5-*exo*-6-tetramethylcyclohexadienyl) iron(II), [Fe(η^5-$C_6H_3Me_4$)$_2$]. This non-carbonyl iron precursor was chosen for its simple synthesis,[13] and is air stable compared to Fe(CO)$_5$. In comparison to the precursor previously reported by our group, this compound has a symmetrical structure and is found to decompose more rapidly, producing iron nanoparticles with a relatively short reaction time.

The Fe precursor was synthesized according to literature methods,[13] and the precursor structure and iron nanoparticle synthesis are outlined in Scheme 1. Briefly, Fe(η^5-$C_6H_3Me_4$)$_2$ is thermally decomposed *via* instant hot injection at 300 °C in octadecene (ODE) with the presence of oleylamine (OLA) as a stabilizing agent. Upon injection, the temperature immediately dropped to 260 °C, and the reaction was maintained at this temperature for 2 h, before cooling to room temperature.

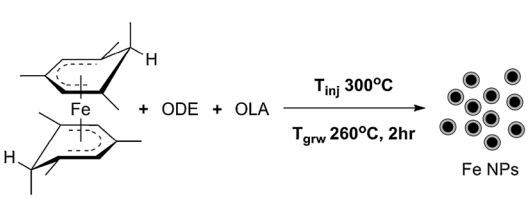

Scheme 1 Structure of iron precursor bis(η^5-1,3,5-*exo*-6-tetramethylcyclohexadienyl) iron(II), [Fe(η^5-$C_6H_3Me_4$)$_2$], and iron/iron oxide core/shell nanoparticle synthesis reaction scheme.

[a] *School of Chemical and Physical Sciences and The MacDiarmid Institute of Advanced Materials and Nanotechnology, Victoria University of Wellington, P.O. Box 600, Wellington, New Zealand. E-mail: richard.tilley@vuw.ac.nz*
[b] *Malaghan Institute of Medical Research, P.O. Box 7060, Wellington, New Zealand*
[c] *Industrial Research Limited, P.O. Box 31-310, Lower Hutt, New Zealand*

† Electronic supplementary information (ESI) available: Materials and methods for nanoparticle synthesis and supporting TEM images, size-distributions and relaxivity data. See DOI: 10.1039/c1cc13416g

Once cooled, the nanoparticles were then isolated from the reaction mixture *via* magnetic separation and washed twice with toluene to remove excess OLA. The purification was done under ambient conditions and the exposure to air at this point leads to the surface oxidation forming iron/iron oxide core/shell nanoparticles. To render the nanoparticles water soluble, the stabilizing agent (OLA) was exchanged with dimercaptosuccinic acid (DMSA). DMSA was chosen due to ease of exchange with OLA due to the strong binding carboxylic acid groups,[14] and its excellent safety profile.[15] The DMSA-coated nanoparticles were readily dispersed in water and the core/shell structures were re-examined six months later by TEM and were found to be identical and the core/shell morphology maintained (Fig. S1).

A typical low magnification transmission electron microscopy (TEM) image of the nanoparticles obtained is shown in Fig. 1A. The nanoparticles are relatively monodisperse, with an average size of 14.0 ± 1.9 nm and with an average core size of 8.5 ± 2.5 nm and a shell with width of 2.9 ± 1.2 nm (calculated from 1000 nanoparticles, Fig. S2) obtained by analysis of TEM images The contrast of the nanoparticles show a darker core surrounded by a lighter shell that reveals a core/shell structure. High-resolution TEM (HRTEM) shows uniform lattice fringes across the entire core with spacings that correspond to α-Fe{211} indicating a single crystal α-Fe core (Fig. 1B). The nanoparticle shell is polycrystalline with multiple domains with various sections corresponding to the {220} planes of iron oxide. The selected area electron diffraction (SAED) of the nanoparticles in Fig. 1A is shown in Fig. 1C and the most intense rings can be indexed to the (110), (200) and (211) reflections of *bcc* α-Fe. An X-ray diffraction pattern of the nanoparticles is shown in Fig. 1D and can be readily indexed to α-Fe and iron oxide peaks (*) corresponding to either magnetite (Fe_3O_4) or maghemite (γ-Fe_2O_3). The average crystallite size of the α-Fe core calculated using the Scherrer equation from the peak width of Fe(110) and Fe(211) is estimated to be 8.7 ± 1.6 nm. This value is consistent with TEM images. The XRD pattern shows broader iron oxide peaks compared to the α-Fe peaks indicating a smaller average crystallite size compared to α-Fe, and is consistent with a polycrystalline shell layer.

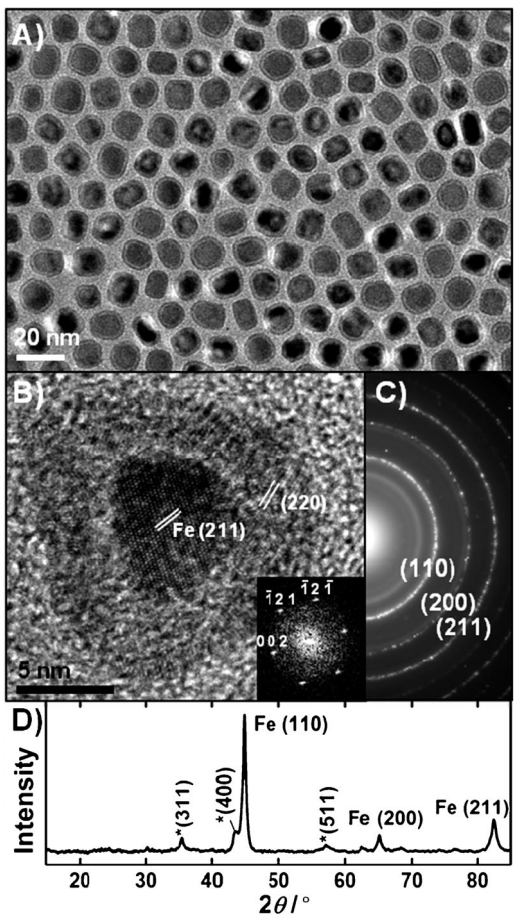

Fig. 1 (A) Low magnification TEM image of iron/iron oxide core/shell nanoparticles. (B) HRTEM showing single crystal α-Fe core with (211) planes observed across core area, and a polycrystalline iron oxide shell with (220) planes observed in sections of shell (inset) corresponding indexed FFT of the α-Fe core viewed down [2,1,0] zone axis. (C) SAED of iron/iron oxide core/shell nanoparticles. (D) XRD pattern of the iron/iron oxide core/shell nanoparticles, with diffraction peaks indexed to α-Fe and spinel iron oxide phase (*).

Magnetic measurements were carried out on the core/shell nanoparticles at 300 K (Fig. 2). The magnetization curve intercepts at the origin, indicating an absence of both a remnant magnetization (M_R) and coercivity (H_C) showing that nanoparticles have superparamagnetic behaviour (inset Fig. 2).[6] The saturated magnetization of 148 emu g^{-1} (Fe) is consistent with previously reported magnetization values for iron/iron oxide core/shell nanoparticles of similar size.[16] The presence of an α-Fe core in the sample induces a higher magnetization compared to pure iron oxide nanoparticles that typically have magnetization values ranging from 40–70 emu g^{-1} (Fe).[2b,17]

To assess effectiveness of the core/shell nanoparticles at enhancing T_2-weighted MR signal the contrast was compared to iron oxides nanoparticles. The iron oxide nanoparticles of similar size (15 ± 2 nm) were synthesized according to literature[18] and coated with DMSA. Both nanoparticles were independently dispersed in agar at varying concentrations of iron (in μg(Fe) mL^{-1}). The core/shell nanoparticles showed an improved negative contrast (darkening) compared to the oxide nanoparticles (Fig. 3A) at iron concentrations of 2.0 to 10.0 μg(Fe) mL^{-1}. The core/shell nanoparticles also showed

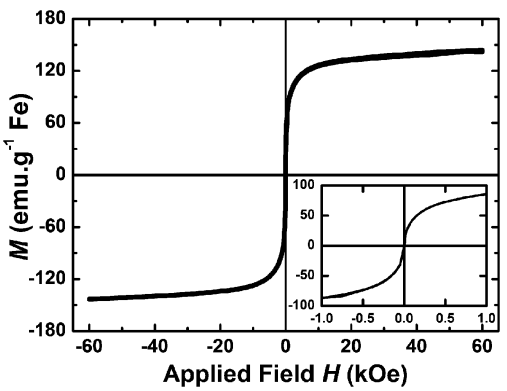

Fig. 2 Magnetization curve of iron/iron oxide core/shell nanoparticles at 300 K, with inset showing the low-field region.

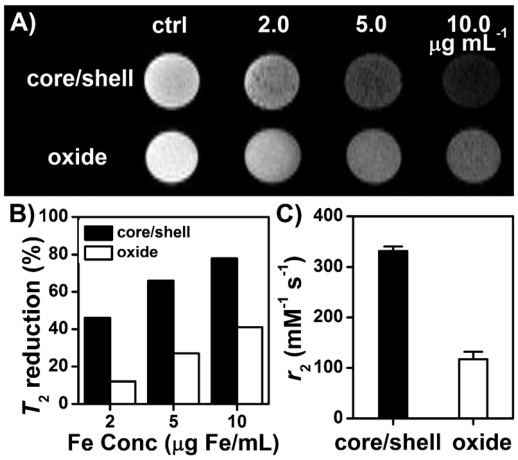

Fig. 3 (A) T_2-weighted MR images at 9.4 T comparing the T_2 contrast (darkening) from core/shell and oxide nanoparticles in agar with concentration of 0.0 (control), 2.0, 5.0 and 10.0 μg(Fe) mL^{-1}. (B) Bar graph comparing the % reduction of T_2 signal relative to that of control caused by core/shell and oxide nanoparticles. (C) Relaxivity (r_2) of the core/shell and oxide nanoparticles determined from the same sample.

greater percent in T_2 signal reduction (relative to that of the control) compared to that of the oxide. The core/shell nanoparticles reduced the T_2-weighted signal by 46, 66 and 78% at 2.0, 5.0 and 10.0 μg(Fe) mL^{-1}, respectively, compared to that of iron oxides, which reduced the T_2-weighted signal by 12, 27 and 41%, respectively, at identical iron concentrations (Fig. 3B). The transverse relaxivity (r_2) of the iron/iron oxide core/shell nanoparticles was determined and compared with the r_2 of iron oxides (see Fig. S3, for plot of T_2 *vs.* [Fe]). The core/shell nanoparticles had an r_2 of 332 mM^{-1} s^{-1}, nearly three-fold larger than that for iron oxide nanoparticles of 117 mM^{-1} s^{-1} (Fig. 3C). This is in agreement with the relaxivity of iron/iron oxide core/shell nanoparticles of similar size.[12] T_2 contrast enhancement of amorphous based iron core/shell nanoparticles relative to iron oxide nanoparticles have previously been reported, however little improvement in r_2 was observed.[19] The large increase in r_2 shown by our iron/iron oxide core/shell nanoparticles indicates the importance of having a single-crystal α-Fe core present, and indicates a significant improvement of the MR signal that will enable greater detection at lower concentrations of iron compared to iron oxides.

Superparamagnetic iron/iron oxide core/shell nanoparticles were synthesized by a simple hot-injection method by decomposing an easy to handle iron organometallic precursor, $Fe(\eta^5\text{-}C_6H_3Me_4)_2$. Surface exchange with DMSA made the core/shell nanoparticles water soluble. The presence of a single-crystalline α-Fe core is shown to produce much greater negative contrast compared to pure iron oxide nanoparticles in T_2-weighted MR imaging, and greatly improved the transverse relaxivity, which will contribute to further developments in magnetic resonance imaging and the next generation of contrast agents.

R.D.T, D.A.J.H, C.D.L and S.P. thank the Foundation of Research, Science and Technology (FRST) for funding through grants PROJ-13733-NMTS, CONT-20568-TTP, CONT-20707-NMTS-IRL and AMP for funding.

Notes and references

1 (*a*) N. Tran and T. J. Webster, *J. Mater. Chem.*, 2010, **20**, 8760–8767; (*b*) R. Hao, R. Xing, Z. Xu, Y. Hou, S. Gao and S. Sun, *Adv. Mater.*, 2010, **22**, 2729–2742; (*c*) Q. A. Pankhurst, N. K. T. Thanh, S. K. Jones and J. Dobson, *J. Phys. D: Appl. Phys.*, 2009, **42**, 224001; (*d*) J.-s. Choi, H.-J. Choi, D.-C. Jung, J.-H. Lee and J. Cheon, *Chem. Commun.*, 2008, 2197–2199.
2 (*a*) T. D. Schladt, K. Schneider, H. Schild and W. Tremel, *Dalton Trans.*, 2011; (*b*) H. B. Na, I. C. Song and T. Hyeon, *Adv. Mater.*, 2009, **21**, 2133–2148.
3 H. B. Na, J. H. Lee, K. J. An, Y. I. Park, M. Park, I. S. Lee, D.-H. Nam, S. T. Kim, S.-H. Kim, S.-W. Kim, K.-H. Lim, K.-S. Kim, S.-O. Kim and T. Hyeon, *Angew. Chem., Int. Ed.*, 2007, **46**, 5397–5401.
4 (*a*) E. Amstad, M. Textor and E. Reimhult, *Nanoscale*, 2011, DOI: 10.1039/c1nr10173k; (*b*) C.-C. Huang, K.-Y. Chuang, C.-P. Chou, M.-T. Wu, H.-S. Sheu, D.-B. Shieh, C.-Y. Tsai, C.-H. Su, H.-Y. Lei and C.-S. Yeh, *J. Mater. Chem.*, 2011, **21**, 7472–7479; (*c*) S. Laurent, D. Forge, M. Port, A. Roch, C. Robic, L. V. Elst and R. N. Muller, *Chem. Rev.*, 2008, **108**, 2064–2110.
5 (*a*) J.-H. Lee, Y.-M. Huh, Y.-w. Jun, J.-w. Seo, J.-t. Jang, H.-T. Song, S. Kim, E.-J. Cho, H.-G. Yoon, J.-S. Suh and J. Cheon, *Nat. Med.*, 2007, **13**, 95–99; (*b*) Y.-w. Jun, Y.-M. Huh, J.-s. Choi, J.-H. Lee, H.-T. Song, KimKim, S. Yoon, K.-S. Kim, J.-S. Shin, J.-S. Suh and J. Cheon, *J. Am. Chem. Soc.*, 2005, **127**, 5732–5733.
6 A.-H. Lu, E. L. Salabas and F. Schuth, *Angew. Chem., Int. Ed.*, 2007, **46**, 1222–1244.
7 D. L. Huber, *Small*, 2005, **1**, 482–501.
8 S. Peng, C. Wang, J. Xie and S. H. Sun, *J. Am. Chem. Soc.*, 2006, **128**, 10676–10677.
9 C. M. Wang, D. R. Baer, L. E. Thomas, J. E. Amonette, J. Antony, Y. Qiang and G. Duscher, *J. Appl. Phys.*, 2005, **98**, 094308.
10 (*a*) H. Lee, T.-J. Yoon and R. Weissleder, *Angew. Chem., Int. Ed.*, 2009, **48**, 5657–5660; (*b*) M. A. Willard, L. K. Kurihara, E. E. Carpenter, S. Calvin and V. G. Harris, *Int. Mater. Rev.*, 2004, **49**, 125–170.
11 (*a*) A. Shavel, B. Rodriguez-Gonzalez, M. Spasova, M. Farle and L. M. Liz-Marzan, *Adv. Funct. Mater.*, 2007, **17**, 3870–3876; (*b*) F. Dumestre, B. Chaudret, C. Amiens, P. Renaud and P. Fejes, *Science*, 2004, **303**, 821–823; (*c*) L.-M. Lacroix, S. Lachaize, A. Falqui, M. Respaud and B. Chaudret, *J. Am. Chem. Soc.*, 2009, **131**, 549–557; (*d*) T. Hyeon, *Chem. Commun.*, 2003, 927–934.
12 S. Cheong, P. Ferguson, K. W. Feindel, I. F. Hermans, P. T. Callaghan, C. Meyer, A. Slocombe, C.-H. Su, F.-Y. Cheng, C.-S. Yeh, B. Ingham, M. F. Toney and R. D. Tilley, *Angew. Chem., Int. Ed.*, 2011, **50**, 4206–4209.
13 M. D. Clerk, M. J. Zaworotko, B. Borecka, T. S. Cameron, D. L. Hooper and A. Linden, *Can. J. Chem.*, 1990, **68**, 1923–1931.
14 A. L. Miller, *Altern. Med. Rev.*, 1998, **3**, 199–207.
15 J. J. Chisolm, *Clin. Toxicol.*, 2000, **38**, 365–375.
16 (*a*) D. Farrell, S. A. Majetich and J. P. Wilcoxon, *J. Phys. Chem. B*, 2003, **107**, 11022–11030; (*b*) C. H. Griffiths, M. P. Ohoro and T. W. Smith, *J. Appl. Phys.*, 1979, **50**, 7108–7115.
17 J. H. L. Beal, S. Prabakar, N. Gaston, G. B. Teh, P. G. Etchegoin, G. Williams and R. D. Tilley, *Chem. Mater.*, 2011, **23**, 2514–2517.
18 T. R. Pisanic, J. D. Blackwell, V. I. Shubayev, R. R. Finones and S. Jin, *Biomaterials*, 2007, **28**, 2572–2581.
19 C. G. Hadjipanayis, M. J. Bonder, S. Balakrishanan, X. Wang, H. Mao and G. C. Hadjipanayis, *Small*, 2008, **4**, 1925–1929.